THE ASTROPHYSICAL JOURNAL, 373:543–555, 1991 June 1

SUPERNOVA REMNANT EVOLUTION IN AN INTERSTELLAR MEDIUM WITH EVAPORATING CLOUDS

RICHARD L. WHITE
Space Telescope Science Institute, 3700 San Martin Drive, Baltimore, MD 21218
AND
KNOX S. LONG[1]
Center for Astrophysical Sciences, Department of Physics and Astronomy, The Johns Hopkins University, Baltimore, MD 21218
Received 1990 June 25; accepted 1990 November 15

ABSTRACT

We have found a new similarity solution that describes the evolution of a supernova remnant expanding into a cloudy interstellar medium. The solution incorporates a reasonable model of the conductive evaporation of cold clouds embedded in the hot gas behind the shock. The conduction is assumed to be saturated in the evaporative flows around the clouds, which is the case for most supernova remnants (SNRs) younger than $\sim$20,000 years old; previous analytical solutions to this problem are only applicable to remnants older than those usually observable at X-ray, optical, and radio wavelengths. The model has two new parameters in addition to those describing the usual Sedov solution for a uniform interstellar medium. We calculate the X-ray, infrared, and optical luminosities of remnants with evaporating clouds, and we also discuss some of the expected spectral characteristics in the various wavebands. Plausible choices for the model parameters produce remnants that are strikingly different from ordinary shell-like supernova remnants; in particular, the effects described here may explain the class of remnants observed to have centrally peaked X-ray emission and shell-like radio emission. Substantial Hα emission is expected from evaporating clouds, although it may not dominate the total Hα luminosity. We hope to learn more about both supernova remnant evolution and the structure of the interstellar medium from studying this class of remnants.

Subject headings: interstellar: matter — nebulae: supernova remnants — radiation mechanisms

1. INTRODUCTION

The standard picture of a supernova remnant (SNR) expanding into a uniform density interstellar medium (ISM) has three stages (Woltjer 1972): (1) the free-expansion phase, in which mass swept up from the ISM is small compared to the ejected mass from the SN, so that the ejecta are hardly slowed by the ISM and expand at constant velocity (shock radius $r_s \propto t$); (2) the adiabatic (or Sedov) phase, in which the swept-up ISM mass exceeds the ejected mass, so that the remnant gradually slows as it sweeps up more and more mass while conserving the total thermal and kinetic energy ($r_s \propto t^{2/5}$); (3) the radiative (or snowplow) phase, in which radiative losses cause the gas to cool rapidly behind the shock and the expansion of the SNR slows greatly.

The evolution of the SNR in the adiabatic phase is described by the similarity solution found by Sedov (1959) for a point explosion in a cold, homogeneous medium. Chevalier (1982) has also found similarity solutions describing SNR evolution in the free-expansion phase for power-law density distributions in both the ISM and the ejecta, and Cox & Edgar (1983) derived a solution for the case when the electron and ion temperatures are not equal. In a similarity solution, the time and radius dependences of all the dynamical variables of the gas (density, pressure, velocity) separate in a particularly simple way. For the pressure, for example,

$$P(r, t) = P_s(r_s) f(r/r_s) . \quad (1)$$

Here $r_s(t)$ is the radius of the shock and P_s is the pressure at the shock as a function of time. In other words, the radial profile of the pressure (and other parameters) remains constant with time.

These similarity solution models for SNR evolution have been successfully applied to explain the observed properties of a wide variety of SNRs. However, some SNRs, including W44, W49B, 3C 400.2, and W28 (Smith et al. 1985; Pye et al. 1984; Long et al. 1990), have centrally peaked X-ray morphologies in striking contrast to the shell-like morphology predicted by the standard SNR models. In this paper we develop a new similarity solution that describes the evolution of a SNR expanding into a cloudy ISM; Long et al. (1990) have applied this model to 3C 400.2 and W28. The clouds embedded in the ISM are assumed to be cold and dense with a small volume filling factor; however, the total mass in clouds may be comparable to or larger than the mass in the intercloud medium (ICM). The shock propagates rapidly through the ICM, leaving behind the clouds. These cold clouds gradually evaporate by saturated conductive heating from the hot, postshock gas (Cowie & McKee 1977, hereafter CM). Although some simplifying assumptions must be made about the cloud evaporation rate for a similarity solution to exist, these assumptions are surprisingly realistic for SNRs with ages between $t \sim 10^3$ and $\sim 2 \times 10^4$ yr and are in reasonable agreement with the cloud evaporation rates estimated by CM. These models can produce SNRs that are similar in appearance to the observed SNRs with centrally peaked X-ray morphologies and limb brightened radio emission.

McKee & Ostriker (1977) also proposed a similarity solution for a SNR with evaporating clouds. Their solution assumed that the

[1] Postal address: Space Telescope Science Institute.

clouds evaporate via classical conduction, so it is applicable to older SNRs ($t > \sim 2 \times 10^4$ yr). Their model is rather different from ours—for example, their SNRs expand with radius $R \propto t^{3/5}$, while our solution has $R \propto t^{2/5}$ like the standard Sedov solution. Chièze & Lazareff (1981) derived the full similarity solution for the case of classical conduction. They showed that for the solution to exist, the intercloud medium density must decline with radius as $R^{-5/3}$. This unphysical assumption is not too important for older SNRs since the density inside such remnants is completely dominated by evaporating clouds, but for younger remnants it may limit the applicability of the Chièze and Lazareff solution.

Ostriker & McKee (1988) also derived analytical expressions describing the evolution of evaporative SNRs. They also emphasized older remnants in which classical conduction is appropriate, although they did briefly discuss saturated conduction. Their methods can be applied to any power-law dependence of the evaporation rate on density, temperature, and radius, but it assumes that the interior structure of the SNR can be described by power-laws in the radius and so is less useful for studying the internal structure of SNRs than are the similarity solutions.

Cowie, McKee, & Ostriker (1981, herafter CMO) performed numerical simulations of the evolution of SNRs in a cloudy ISM with a quite detailed model of the physics of evaporation, including the saturation of conduction. Their results confirmed the similarity solution of McKee & Ostriker (1977) for older SNRs. We shall show below that their calculations for younger SNRs (in what they call the "adolescent" phase, $10^3 < t < 2 \times 10^4$ yr, $5 < R < 20$ pc) are in reasonable agreement with the similarity solution we present here.

In the remainder of this paper, we derive the similarity solution for a SNR in a cloudy ISM (§ 2), discuss the observable properties of an evaporation-dominated SNR in the X-ray, infrared, and optical (§ 3), and summarize our results (§ 4).

2. SIMILARITY SOLUTION

2.1. *Hydrodynamic Equations with Evaporating Clouds*

Consider the dynamical evolution of an explosion in a cloudy medium. We assume that (1) the explosion is spherically symmetric, (2) the intercloud medium (ICM) is homogeneous and uniform, (3) clouds are much denser than the intercloud medium, (4) the clouds are numerous and are uniformly distributed, but (5) the filling factor of the clouds is small. With these assumptions, little energy is deposited directly into the clouds by the shock; they are neither accelerated nor heated significantly by the shock. Instead, the shock propagates around the clouds through the ICM, leaving behind the clouds, still cold and at rest, embedded in the hot, high-speed postshock gas. The dense cloud material is then evaporated and ablated so that it mixes with the ICM in the postshock gas.

The gas boiling off the clouds is a source of mass for the ICM, but it initially has no energy or momentum. The momentum and energy of the ICM must be used to bring the cold cloud gas up to the temperature and velocity of the ICM; this cools and slows the ICM gas. The hydrodynamic equations for the evolution of the SNR are then

$$\frac{\partial \rho}{\partial t} + \frac{1}{r^2}\frac{\partial}{\partial r}(r^2 v \rho) = j \,, \tag{2a}$$

$$\frac{\partial v}{\partial t} + v\frac{\partial v}{\partial r} + \frac{1}{\rho}\frac{\partial P}{\partial r} = -\frac{v}{\rho} j \,, \tag{2b}$$

$$\frac{\rho^\gamma}{P}\frac{d}{dt}\left(\frac{P}{\rho^\gamma}\right) = \frac{j}{\rho}\left[\frac{1}{2}(\gamma - 1)\frac{\rho v^2}{P} - \gamma\right], \tag{2c}$$

where ρ, v, and P are the ICM density, velocity, and pressure, and j is the integrated cloud evaporation rate (g cm^{-3} s^{-1}). The energy equation assumes adiabatic flow with an adiabatic index γ, with no radiative losses or internal shocks. The boundary conditions for the solution are determined by the jump conditions at the ISM shock. If the ISM is cold,

$$\rho_s = \frac{\gamma + 1}{\gamma - 1}\rho_1 \,, \tag{3a}$$

$$P_s = \frac{2\rho_1 V_s^2}{\gamma + 1} \,, \tag{3b}$$

$$v_s = \frac{2}{\gamma + 1} V_s \,, \tag{3c}$$

where ρ_1 is the density of the ICM to the undisturbed ISM and V_s is the shock velocity.

2.2. *Similarity Equations*

To find a similarity solution, we make the following substitutions:

$$x = r/r_s \,; \quad P = P_s f(x) \,; \quad f(1) = 1 \,; \quad \rho = \rho_s g(x) \,; \quad g(1) = 1 \,; \quad v = V_s h(x) \,;$$
$$h(1) = 2/(\gamma + 1) \,; \quad j = j_s k(x) \,. \tag{4}$$

As for the usual Sedov (1959) solution, the dependence of P_s, V_s, and ρ_s on r_s is determined by the requirement that the r_s dependence

drop out of the resulting ordinary differential equations:

$$P_s = \frac{KE}{2\pi r_s^3}, \tag{5}$$

$$V_s = \left[\frac{(\gamma+1)KE}{4\pi\rho_1 r_s^3}\right]^{1/2}, \tag{6}$$

where E is the energy of the explosion and

$$K = (\gamma-1)\Big/\int_0^1 x^2\,dx[2f + \tfrac{1}{2}(\gamma+1)^2 gh^2] \tag{7}$$

is a dimensionless constant that determines the ratio of thermal to kinetic energy in the SNR. Integrating $V_s = dr_s/dt$ gives

$$r_s = \left[\frac{25(\gamma+1)KE}{16\pi\rho_1}\right]^{1/5} t^{2/5}. \tag{8}$$

The scaling of all these variables is exactly the same as for the standard Sedov solution without evaporating clouds, although the value of the constant K differs when evaporation is included.

The resulting ordinary differential equations for f, g, and h are

$$(h-x)g' + gh' = Ak - \frac{2gh}{x} \tag{9a}$$

$$\frac{2(\gamma-1)}{(\gamma+1)^2} f' + g(h-x)h' = h\left(\frac{3}{2}g - Ak\right) \tag{9b}$$

$$g(h-x)f' - \gamma f(h-x)g' = 3fg + Ak\left[\frac{(\gamma+1)^2}{4} gh^2 - \gamma f\right] \tag{9c}$$

where

$$A = j_s r_s / V_s \rho_s. \tag{10}$$

2.3. *Scaling of the Evaporation Rate*

For a similarity solution to exist, A must be a constant. This implies that the evaporation rate at the shock

$$j_s = A\frac{\rho_s V_s}{r_s} = A\rho_s \frac{d(\ln r_s)}{dt} = A\frac{2\rho_s}{5t}. \tag{11}$$

Since ρ_s is constant, we must have $j_s \propto 1/t$.

There is no reason we should expect the real cloud evaporation rate to scale in just the way that is required to allow a similarity solution to exist; however, the scaling in equation (11) is, in fact, astoundingly close to that expected under a variety of assumptions if the electron conduction is saturated, which is usually the case in SNRs until they reach the age of 2×10^4 yr (Cowie 1977; CMO). For example, CM have calculated the evaporation rate for spherical clouds embedded in a hot medium. They find that the saturated evaporation rate for a single cloud is

$$\dot{m}_c \propto \{\rho^5 T^{5[1+(1/2)M_s^2]} R_c^{11+M_s^2}\}^{1/(6+M_s^2)}, \tag{12}$$

where ρ and T are the temperature and density for the hot medium, R_c is the cloud radius, and M_s is a Mach number that depends on the efficiency of saturated conduction (more on M_s below). To get j from $\dot{m}_c$ we just multiply by the number of clouds per unit volume N_c [or integrate over $N_c(R_c)$ if there is a size distribution].

At the shock, ρ_s = constant and $T_s \propto V_s^2 \propto t^{-6/5}$. If we assume that N_c and R_c are constant, then

$$j_s \propto t^{-[1+(1/2)M_s^2]/[1+(1/6)M_s^2]}. \tag{13}$$

In order to have $j_s \propto t^{-1}$ we evidently must have $M_s^2 \ll 1$. In the absence of magnetic fields $M_s^2 \simeq 2$ (CM), and hence $j_s \propto t^{-3/2}$, but the expected magnetic fields can reduce M_s^2 substantially. CM use values of M_s^2 as small as 0.2, which would make $j_s \propto t^{-1.06}$.

If we include the effects of cloud compression in the high pressure gas inside the SNR, the scaling of the evaporation rate is close to t^{-1} even when magnetic fields do not inhibit the evaporation. To derive equation (13) we assumed that R_c is constant just behind the shock; in reality, however, the clouds get compressed by the hot gas behind the shock and R_c depends on P_s. Suppose that the cloud pressure $P_c \propto P_s$ and that the cloud is compressed adiabatically so $P_c \propto \rho_c^{\gamma_c}$. Then $R_c \propto P_s^{-1/3\gamma_c}$ and

$$j_s \propto t^{-[1-(11/15\gamma_c)+M_s^2 1/2(-1/15\gamma_c)]/[1+(1/6)M_s^2]}. \tag{14}$$

If the cloud does not cool as it is compressed then $\gamma_c = 5/3$ and $j_s \propto t^{-1.11}$ assuming $M_s^2 = 2$. If the cloud cools strongly and remains isothermal as it is compressed, then $\gamma_c = 1$ and $j_s \propto t^{-0.85}$. If the cloud is supported by magnetic fields, then $\gamma_c = 2$ and $j_s \propto t^{-1.18}$.

In the latter case, one would expect the magnetic fields to reduce the efficiency of the conduction somewhat; for example, if $M_s^2 = 1$ then $j_s \propto t^{-0.94}$ for a magnetically supported cloud. In every case the scaling of the evaporation rate is quite close to the t^{-1} required for a similarity solution.

How close must the evaporation rate scaling be to $1/t$ in order for the similarity solution to be applicable? Suppose the real evaporation rate scales roughly as $j_{s,r} \propto 1/t^{1+\epsilon}$ for some period of time $t_1 < t < t_2$. If we use the evaporation rate scaling $j_s = j_{s,r}(\bar{t})\bar{t}/t$, where $\bar{t} = (t_1 t_2)^{1/2}$, then the fractional error in our evaporation rate is less than $(t_2/t_1)^{\epsilon/2} - 1$ for $t_1 < t < t_2$. As an example, if $t_2/t_1 = 10$ then the error that results from assuming $j_s \propto 1/t$ is only $\pm 25\%$ for real scaling laws with $j_s \propto 1/t^{1\pm 0.2}$ as implied by equation (14). In other words, as the remnant ages by an order of magnitude, and the evaporation rate j_s also changes by an order of magnitude, the simple evaporation rate will be correct to within 25% if the power law of the actual scaling is within 0.2 of -1.

The complete physics of cloud evaporation is rather complicated; other effects such as heating by shocks driven into the cloud (Sgro 1975), ablation by the high-speed, hot gas behind the shock, and bulk acceleration by the ram pressure of that gas may be important. CMO have calculated numerical models for SNR evolution which include many of these other effects as well as an accurate description of the conductive evaporation. They find that for SNRs with $10^3 < t < 2 \times 10^4$ yr the mean density $\langle\rho\rangle$ inside the remnant is dominated by the evaporated material but is constant with time. That is exactly what $j_s \propto 1/t$ implies! The requirement that the evaporation rate must scale as $1/t$ comes directly from the requirement that ρ_s and therefore $\langle\rho\rangle$ is constant with time (eq. 11). If $j_s \propto 1/t^{1+\epsilon}$ then the mean density of evaporated gas in a SNR would decrease as $R^{-5\epsilon/2}$. From Figure 5 of CMO, $0 < \epsilon < \sim 0.15$ for $t < 2 \times 10^4$ yr; this implies that the evaporation rate assuming $j_s \propto 1/t$ is in error by less than 25% between $10^3 < t < 2 \times 10^4$ yr. Thus, the detailed numerical simulations of CMO provide strong support for $j_s \propto 1/t$.

In summary, it is clear that the scaling that is required for a similarity solution to exist does lie within the range of reasonable physical models for the evaporation of clouds embedded in SNRs with ages from 10^3 to 2×10^4 yr. This gives us confidence that the similarity solution will not differ greatly from the solution that could be calculated using the complete physics of evaporation.

2.4. *Adopted Evaporation Rate*

The complexity of evaporation suggests that one should not rely too much on the fine details of CM's evaporation rate. We adopt here a simple form for the evaporation rate suggested by equation (12):

$$\dot{m}_c = \frac{m_c}{t_{\rm evap}} \left(\frac{P}{P_s}\right)^{5/6}, \tag{15}$$

where m_c is the cloud mass and $t_{\rm evap} = rt$ sets the evaporation time scale. The dimensionless constant τ is the ratio of the time to evaporate a cloud to the age of the SNR. For $\tau \gg 1$, clouds evaporate slowly; for $\tau \ll 1$, clouds evaporate quickly after passing through the shock front.

The biggest advantage of this form for $\dot{m}_c$ is that the total evaporation rate j is then independent of the cloud size distribution:

$$j = \int dm_c\, N_c(m_c)\dot{m}_c = \frac{\rho_c}{t_{\rm evap}} \left(\frac{P}{P_s}\right)^{5/6}, \tag{16}$$

where $\rho_c = \int dm_c\, m_c\, N_c(m_c)$ is the contribution of clouds to the mean density of the ISM, i.e., the density the clouds would have if they were dispersed and distributed uniformly in space.

At the shock $\rho_c = \rho_{c1}$ is determined by the cloudy structure of the undisturbed ISM. As the clouds evaporate, $d\rho_c/dt = -j$ and the fraction of cloud mass remaining

$$l(x) = \frac{\rho_c(x)}{\rho_{c1}} = \exp\left[-\frac{5}{2\tau}\int_x^1 \frac{dx}{x} f(x)^{5/6}\right], \tag{17}$$

with

$$k(x) = l(x) f(x)^{5/6}, \tag{18}$$

$$A = \frac{5}{2\tau}\frac{\rho_{c1}}{\rho_s} = \frac{5C}{2\tau}\frac{\gamma - 1}{\gamma + 1}, \tag{19}$$

where $C = \rho_{c1}/\rho_1$. The quantity $l(x)$ is most conveniently calculated if it is expressed as a differential equation,

$$l' = \frac{5}{2\tau}\frac{l f^{5/6}}{x}, \qquad l(1) = 1. \tag{20}$$

If the evaporation rate scales roughly but not exactly as $1/t$, we expect the true solution to resemble the similarity solution, drifting slowly through the solutions for various values of the parameters C and τ. For example, when a SNR is young the evaporation time τt might be long compared to the age t so that the solution would look like the standard Sedov model (or more realistically like the solutions found by Chevalier 1982); as the SNR ages, τ might decrease, leading to a SNR whose morphology is dominated by the effects of evaporation. As long as the scaling of the true evaporation rate crudely resembles our adopted form, we expect the similarity solution to be robust and applicable to real SNRs.

We would like to emphasize that the evaporation rate given in equation (15) is not the only one for which a similarity solution exists. The only requirement is that j_s scale as $1/t$; any combination of the physical variables that satisfies that requirement is acceptable. In particular, it is possible to include the effects of changing evaporation rate as a function of cloud size so that some

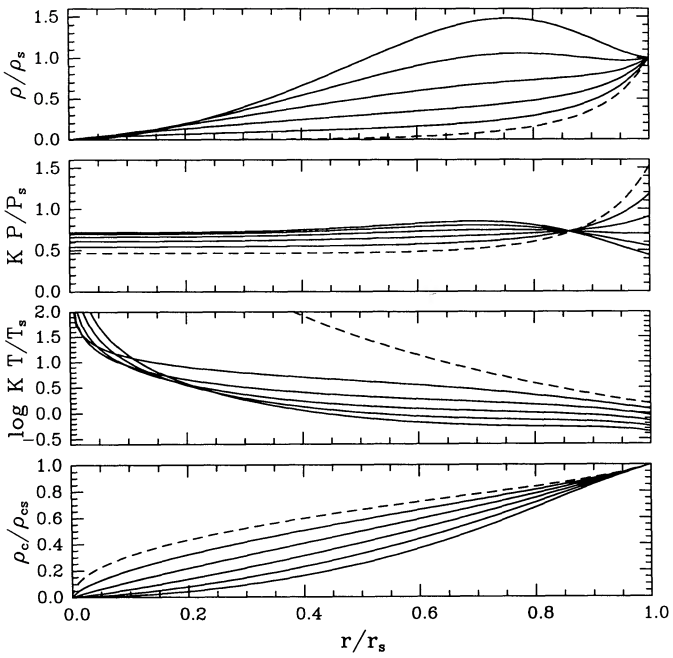

FIG. 1a

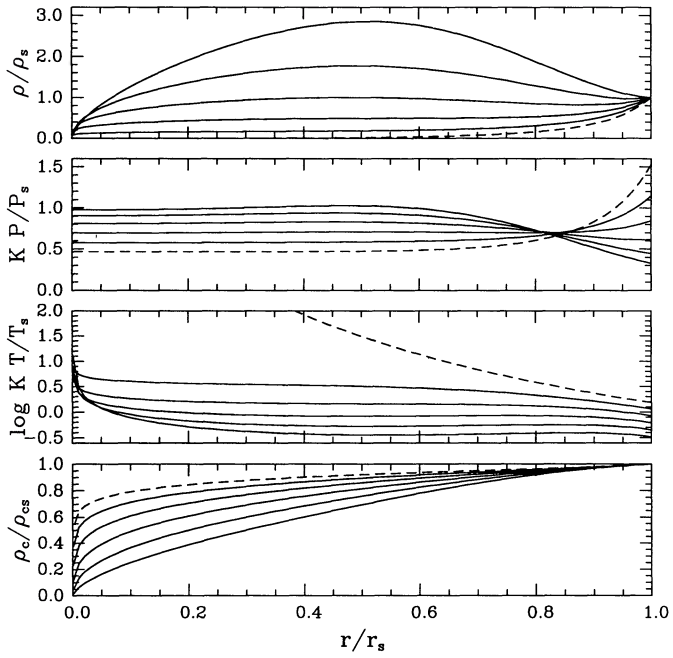

FIG. 1b

FIG. 1.—Dimensionless density, pressure, log temperature, and remaining cloud mass as a function of radius for SNRs with evaporating clouds. (*a*) $\tau = 2$, $C = 0$ (*dashed line*), 2, 4, 6, 8, 10. (*b*) $\tau = 10$, $C = 0$ (*dashed line*), 10, 20, 30, 40, 50.

clouds evaporate completely before they reach the center of the SNR. We have chosen the rate used here because it seems the simplest form which includes a reasonable dependence on the state of the ICM without introducing many new parameters to describe the size and mass distribution of the clouds. However, both better evaporation physics and more realistic cloud size distributions can be readily accommodated in the similarity solution.

2.5. *Solutions*

The complete similarity solution can now be found by integrating numerically equations (9a)–(9c) and (18)–(20) from the boundary conditions at $x = 1$ inward toward $x = 0$. The equations are well behaved, so the numerical integration of the equations is straightforward. The model has five parameters, including the three standard Sedov parameters: E (the explosion energy), ρ_1 (the preshock ICM density), and t (the age of the SNR), and two new dimensionless parameters describing the clouds: $C = \rho_{c1}/\rho_1$ (the ratio of ISM mass in clouds to ISM mass in the ICM) and $\tau = t_{\rm evap}/t$ (the ratio of the cloud evaporation time scale to the SNR age).

The two new parameters do increase the range of solutions compared to the Sedov solution, but it is not true (as one might guess) that we now have so many free parameters that we can fit any radial morphology for a SNR. Extreme values of the parameters often lead right back to the Sedov solution. Obviously when $C \ll 1$ the solution approaches the Sedov solution, because the evaporated cloud mass is negligible. When $\tau \gg C$ the evaporated mass is again small and the Sedov solution applies. It may be less obvious that when $\tau \ll 1$, the clouds evaporate so quickly that the solution looks like a Sedov model with an ISM density $\rho_1 + \rho_{c1}$.

Only when $C \gtrsim 1$ and $1 \lesssim \tau \lesssim C$ does the solution with evaporation differ appreciably from a standard Sedov solution. Figure 1 shows how $\rho(r)$, $P(r)$, $T(r)$, and the remaining cloud mass $\rho_c(r)$ vary with the evaporation parameters. We have explicitly included the K dependence of P and T in the figures (eqs. [5] and [7]). This allows the direct comparison of solutions for different parameter values. For example, to convert the dimensionless pressure KP/P_s to the dimensional pressure, simply multiply it by $E/2\pi r_s^3$ (eq. [5]). The values of K for various parameters are given in Table 1; other integration constants of interest, discussed below, are given in

TABLE 1

CONSTANT OF INTEGRATION K/K(Sedov)

C	$\tau = 0.1$	$\tau = 0.2$	$\tau = 0.5$	$\tau = 1.0$	$\tau = 2.0$	$\tau = 5.0$	$\tau = 10.0$	$\tau = 20.0$	$\tau = 50.0$	$\tau = 100.0$
0.5.....	0.708	0.748	0.830	0.893	0.939	0.974	0.986	0.993	0.997	0.999
1.0.....	0.541	0.585	0.695	0.797	0.881	0.948	0.973	0.986	0.994	0.997
2.0.....	0.363	0.398	0.503	0.637	0.775	0.898	0.947	0.973	0.989	0.994
5.0.....	0.179	0.194	0.247	0.350	0.524	0.758	0.870	0.933	0.973	0.986
10.0.....	0.096	0.102	0.123	0.170	0.288	0.566	0.752	0.869	0.946	0.973
20.0.....	0.049	0.052	0.059	0.074	0.118	0.313	0.554	0.749	0.893	0.946
50.0.....	0.020	0.020	0.022	0.025	0.033	0.077	0.215	0.465	0.747	0.867
100.0.....	0.010	0.010	0.011	0.011	0.013	0.023	0.060	0.203	0.544	0.746

NOTE.—For Sedov solution, $K = 1.528$. The age of a SNR scales as $K^{-1/2}$.

Tables 2–5. Note that the age of SNRs with a given radius scales as $K^{-1/2}$ (eq.[8]), so it takes remnants longer to reach a given size when evaporation is important if the ICM density is fixed.

The main effect of evaporation is to increase the density and decrease the temperature in the center of the SNR. For sufficiently large values of C the density may be peaked near the center, although ρ always goes to zero just at the center of the SNR. A secondary effect is that the ratio $P(0)/P_s$ increases as the evaporated mass increases, because evaporation slows the expansion of the remnant, allowing the pressure at the center to remain higher.

TABLE 2

SCALED X-RAY LUMINOSITY Q

C	$\tau = 0.1$	$\tau = 0.2$	$\tau = 0.5$	$\tau = 1.0$	$\tau = 2.0$	$\tau = 5.0$	$\tau = 10.0$	$\tau = 20.0$	$\tau = 50.0$	$\tau = 100.0$
0.5.....	0.864	0.794	0.733	0.742	0.794	0.879	0.929	0.962	0.984	0.992
1.0.....	0.842	0.744	0.629	0.610	0.662	0.784	0.868	0.926	0.968	0.984
2.0.....	0.866	0.762	0.588	0.504	0.515	0.644	0.765	0.861	0.938	0.968
5.0.....	0.960	0.909	0.752	0.565	0.424	0.441	0.565	0.710	0.857	0.923
10.0.....	1.039	1.061	1.049	0.908	0.615	0.372	0.413	0.550	0.747	0.855
20.0.....	1.102	1.192	1.396	1.528	1.342	0.585	0.357	0.399	0.594	0.745
50.0.....	1.155	1.311	1.773	2.465	3.339	2.832	1.029	0.389	0.390	0.537
100.0.....	1.178	1.364	1.961	3.026	5.086	8.038	5.315	1.248	0.346	0.387

NOTE.—Scaled by L_x (Sedov) $[1 + C/(1 + \tau)]^2$, where L_x (Sedov) $= 0.04315\, 4\pi r_s^3\, 10.5 n_1^2\, \Lambda_x$.

TABLE 3

SCALED EMISSION-MEASURE-WEIGHTED TEMPERATURE $\langle T \rangle$

C	$\tau = 0.1$	$\tau = 0.2$	$\tau = 0.5$	$\tau = 1.0$	$\tau = 2.0$	$\tau = 5.0$	$\tau = 10.0$	$\tau = 20.0$	$\tau = 50.0$	$\tau = 100.0$
0.5.....	0.723	0.772	0.862	0.921	0.958	0.983	0.991	0.996	0.998	0.999
1.0.....	0.554	0.610	0.738	0.842	0.916	0.966	0.983	0.991	0.997	0.998
2.0.....	0.370	0.413	0.541	0.693	0.829	0.931	0.966	0.983	0.993	0.997
5.0.....	0.181	0.197	0.257	0.375	0.576	0.819	0.912	0.957	0.983	0.991
10.0.....	0.096	0.102	0.124	0.173	0.300	0.621	0.815	0.911	0.965	0.983
20.0.....	0.049	0.051	0.058	0.073	0.116	0.315	0.603	0.812	0.929	0.965
50.0.....	0.020	0.020	0.022	0.024	0.031	0.070	0.193	0.487	0.811	0.911
100.0.....	0.010	0.010	0.011	0.011	0.013	0.021	0.050	0.171	0.585	0.810

NOTE.—Scaled by Sedov value, $\langle T(\text{Sedov}) \rangle = 1.948 T_s$.

TABLE 4

SCALED X-RAY MASS G

C	$\tau = 0.1$	$\tau = 0.2$	$\tau = 0.5$	$\tau = 1.0$	$\tau = 2.0$	$\tau = 5.0$	$\tau = 10.0$	$\tau = 20.0$	$\tau = 50.0$	$\tau = 100.0$
0.5.....	0.994	0.982	0.952	0.937	0.940	0.962	0.977	0.987	0.995	0.997
1.0.....	0.999	0.987	0.944	0.909	0.902	0.931	0.956	0.975	0.989	0.995
2.0.....	1.011	1.009	0.968	0.905	0.865	0.884	0.921	0.953	0.979	0.989
5.0.....	1.036	1.060	1.079	1.020	0.897	0.823	0.851	0.900	0.951	0.974
10.0.....	1.055	1.101	1.193	1.225	1.098	0.847	0.805	0.842	0.913	0.951
20.0.....	1.070	1.134	1.294	1.460	1.506	1.089	0.838	0.794	0.857	0.912
50.0.....	1.083	1.164	1.387	1.700	2.113	2.155	1.383	0.894	0.788	0.835
100.0.....	1.090	1.178	1.431	1.815	2.448	3.354	2.870	1.486	0.832	0.786

NOTE.—Scaled by M_x(Sedov)$[1 + C/(1 + \tau)]$, where M_x(Sedov) $= 4\pi r_s^3\, \rho_1/3$.

TABLE 5

SCALED Hα LUMINOSITY S

C	$\tau = 0.1$	$\tau = 0.2$	$\tau = 0.5$	$\tau = 1.0$	$\tau = 2.0$	$\tau = 5.0$	$\tau = 10.0$	$\tau = 20.0$	$\tau = 50.0$	$\tau = 100.0$
0.5.....	0.185	0.167	0.122	0.080	0.047	0.020	0.011	0.005	0.002	0.001
1.0.....	0.330	0.306	0.236	0.160	0.094	0.041	0.021	0.011	0.004	0.002
2.0.....	0.551	0.527	0.442	0.320	0.192	0.084	0.043	0.022	0.009	0.004
5.0.....	0.993	0.975	0.903	0.752	0.499	0.219	0.110	0.055	0.022	0.011
10.0.....	1.477	1.463	1.413	1.294	0.997	0.468	0.230	0.112	0.044	0.022
20.0.....	2.147	2.136	2.099	2.021	1.792	1.030	0.501	0.236	0.090	0.044
50.0.....	3.453	3.444	3.417	3.369	3.246	2.629	1.530	0.682	0.240	0.114
100.0.....	4.912	4.905	4.883	4.844	4.759	4.388	3.377	1.683	0.533	0.241

NOTE.—Scaled by $L_{H\alpha} = 5 h\nu_{H\alpha}\, F(X_H/m_H)\, [\pi \rho_1\, r_s(\gamma + 1)E]^{1/2}$; all quantities are explained in § 3.3.

TABLE 6

CONSTANTS OF INTEGRATION FOR ONE-PARAMETER MODELS

C/τ	K/K(Sedov)	Q = Scaled L_x	Scaled $\langle T \rangle$	G = Scaled M_x	S = Scaled $L_{H\alpha}$
0.0.....	1.000	1.000	1.000	1.000	0.000
0.5.....	0.867	0.534	0.910	0.833	0.115
1.0.....	0.746	0.384	0.809	0.784	0.242
1.5.....	0.637	0.337	0.697	0.789	0.384
2.0.....	0.541	0.344	0.580	0.830	0.542
2.5.....	0.457	0.394	0.469	0.898	0.717
3.0.....	0.385	0.490	0.372	0.993	0.911
3.5.....	0.323	0.643	0.292	1.112	1.125
4.0.....	0.270	0.872	0.229	1.260	1.361
5.0.....	0.189	1.685	0.143	1.645	1.906
6.0.....	0.132	3.309	0.091	2.175	2.558
7.0.....	0.093	6.431	0.059	2.884	3.329
8.0.....	0.066	12.229	0.040	3.812	4.232
9.0.....	0.047	22.663	0.027	5.007	5.281
10.0.....	0.034	40.890	0.019	6.526	6.487

NOTE.—All quantities scaled as in Tables 1–5.

In the limit as C and $\tau \to \infty$ the solution depends only on the ratio C/τ. The remaining cloud mass $l(x)$ is then constant (eq. [20]). The values of K (and other integration constants) for a range of C/τ are given in Table 6. Figure 2 shows the solutions for a range of C/τ values. Figure 3 shows how the two-parameter solutions converge to the one-parameter solution for a particular case. All the variables except the density converge very rapidly as C and τ increase; the density differs mainly near the center of the SNR where there is relatively little mass. One can find a one-parameter solution that resembles closely practically any two-parameter solution; consequently, the one-parameter solutions can be quite useful in matching models to observations of specific SNRs.

A comparison of our similarity solutions with the numerical models of CMO shows reasonable agreement in the global properties of the SNRs though there are significant differences in details. The most noticeable difference is that CMO's models include a component of warm, lower density clouds which evaporate completely in the outer part of the SNR. These clouds are also accelerated by the ram pressure of the fast-moving ICM. This leads to an enhanced density in the outer half of the SNRs compared to our models. A modification of the evaporation rate used in the similarity solution, as discussed at the end of § 2.4, would presumably allow the similarity solution to exhibit similar behavior; however, such a model would not agree as well with the X-ray observations as do the models we present in this paper.

3. OBSERVABLE PROPERTIES

McKee (1982) discussed some of the observational properties of SNRs expanding into an evaporative, cloudy ISM. His emphasis was on older SNRs for which the clouds evaporate via classical conduction, though some of his conclusions also apply to any

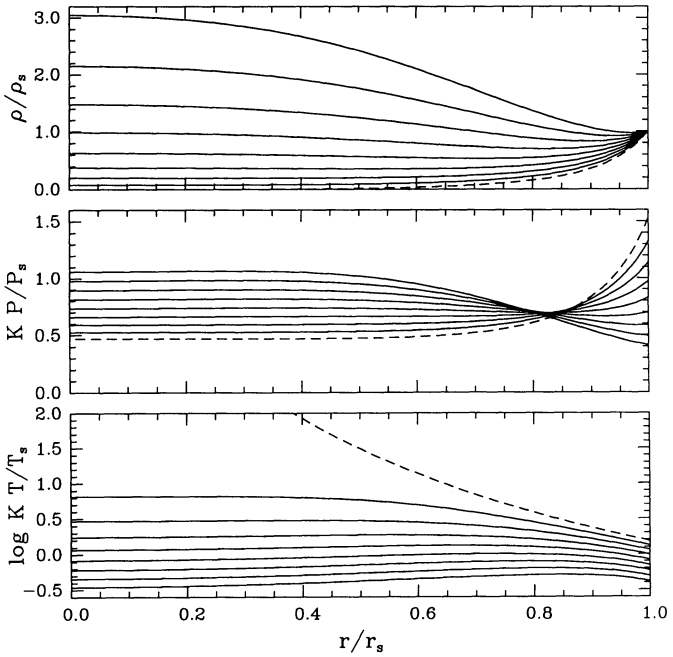

FIG. 2.—Dimensionless density, pressure, and log temperature for models with $\tau \to \infty$. $C/\tau = 0$ (*dashed line*), 0.5, 1.0, 1.5, 2.0, 2.5, 3.0, 3.5, 4.0.

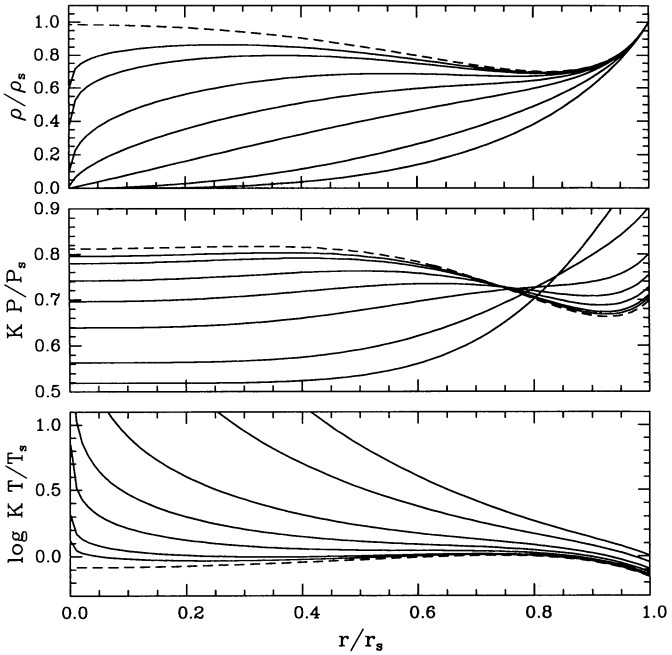

FIG. 3.—Convergence to $\tau \to \infty$ solution. $C/\tau = 2.5$, $C = 1, 2, 5, 10, 20, 50, 100, \infty$ (*dashed line*). Note scale has been expanded on T and P plots.

evaporative SNRs. With the similarity solution derived above, we can learn about some details of the appearance of younger SNRs. Below we discuss the emission in X-rays, infrared, and Hα implied by our model.

3.1. *X-Ray Emission*

SNRs emit much of their radiation in X-rays because of the high temperatures ($T \sim 10^6$–10^8 K) of the postshock gas. Although recent observations indicate that SNRs often radiate more energy in the infrared than in X-rays (Graham et al. 1987; Dwek et al. 1987; see § 3.2 for much discussion), SNRs are still more easily studied at X-ray wavelengths: IR observations are hampered by the bright sky background and by confusion from other nearby astronomical sources, especially in the Galactic plane where most SNRs are found. The details of X-ray emission are somewhat complicated because the X-ray spectrum in the 0.1–10 keV range is formed by a variety of line and continuum processes that depend on the details of the temperatures, densities, ionization structure, and elemental abundances in the hot gas, and on the intervening interstellar absorption as well. Long et al. (1990) compare the models discussed in this paper with X-ray observations of some SNRs; here we will simply describe the qualitative appearance of the X-ray emission from SNRs with evaporating clouds and will make rough estimates of the X-ray luminosities of such SNRs.

The X-ray luminosity and morphology of a SNR are defined mainly by the radial density distribution within the remnant. The temperature distribution is of secondary importance because the variation in $n_e n_H$ is generally larger than the variation in $\Lambda_x(T)$, where the X-ray emissivity per unit volume is $n_e n_H \Lambda_x(T)$. Hamilton, Sarazin, & Chevalier (1983) calculated the X-ray emission from SNRs, including the important effects of nonequilibrium ionization. They found that the 0.1–2 keV X-ray emission from a Sedov SNR is nearly independent of the shock temperature, but instead depends mainly on the ionization time scale parameter nt. In fact, for $nt = 30$–3000 cm^{-3} yr they find that Λ_x is constant to within 50%: $\Lambda_x \simeq 1 \times 10^{-22}$ cm^{-3} ergs s^{-1} (see their eq. [11]). Here we shall use this value of Λ_x to calculate the 0.1–2 keV X-ray luminosity of our SNRs.

If Λ_x is constant, the total X-ray luminosity is

$$L_x = \int_0^{r_s} 4\pi r^2 n_e n_H \Lambda_x(r) dr = 4\pi r_s^3 \, 10.5 n_1^2 \Lambda_x \int_0^1 dx x^2 g(x)^2$$

$$= 3.9 \times 10^{35} \text{ ergs s}^{-1} \left(\frac{r_s}{1 \text{ pc}}\right)^3 n_1^2 \left(\frac{\Lambda_x}{1 \times 10^{-22}}\right) \int_0^1 dx x^2 g(x)^2$$

$$= 1.7 \times 10^{34} \text{ ergs s}^{-1} \left(\frac{r_s}{1 \text{ pc}}\right)^3 n_1^2 \left(\frac{\Lambda_x}{1 \times 10^{-22}}\right) Q \left(1 + \frac{C}{1+\tau}\right)^2 . \quad (21)$$

Here $n_1 = \rho_1/m_H$ is the density of the ICM just outside the shock, and we have used $n_H = 0.75\rho/m_H$ and $n_e = 0.875\rho/m_H$. We have scaled the integral by a simple heuristic model of its dependence on τ and C,

$$\int_0^1 dx x^2 g(x)^2 = 0.4315 Q[1 + C/(1+\tau)]^2,$$

where Q is a number of order 1. The quantity Q is tabulated in Tables 2 and 6. This form for the function has the right behavior in the limits $\tau \to 0$ and $\tau \to \infty$; in the former case clouds evaporate instantly and the effective ISM density is just $(1 + C)\rho_1$, while in the

latter case only a fraction $\sim 1/\tau$ of the cloud mass evaporates. As the table shows, this is a reasonable approximation except for very large values of C/τ and takes out much of the strong dependence of the integral on the parameters.

The X-ray morphology of the SNR is roughly determined by the column emission measure (EM) as a function of impact parameter b in the SNR:

$$\mathrm{EM}(b) = \int_{-\sqrt{r_s^2 - b^2}}^{\sqrt{r_s^2 - b^2}} d\,ln^2(r)\,, \qquad r^2 = b^2 + l^2 = 2n_s^2 r_s \left[\int_{b/r_s}^{1} \frac{dx x g(x)^2}{\sqrt{x^2 - (b/r_s)^2}} \right]. \tag{22}$$

Figure 4 shows how the emission measure varies as a function of the model parameters for the same solutions displayed in Figures 1

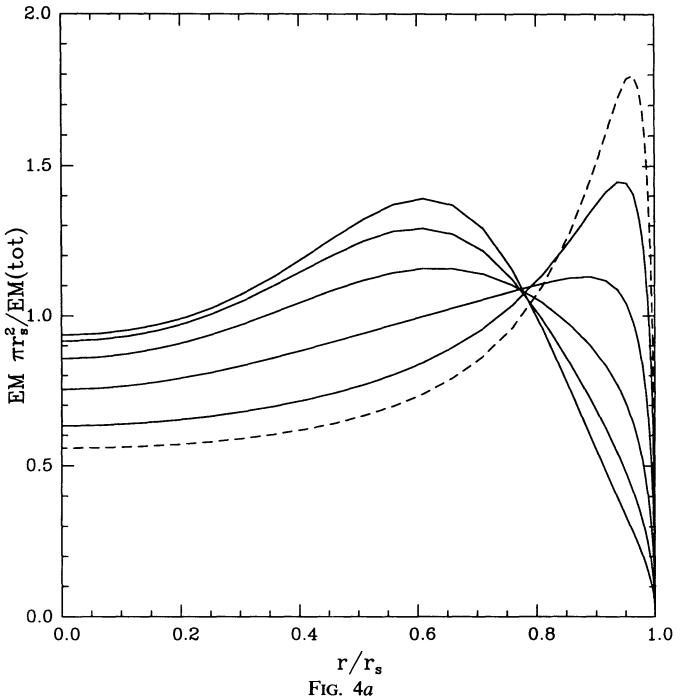

FIG. 4*a*

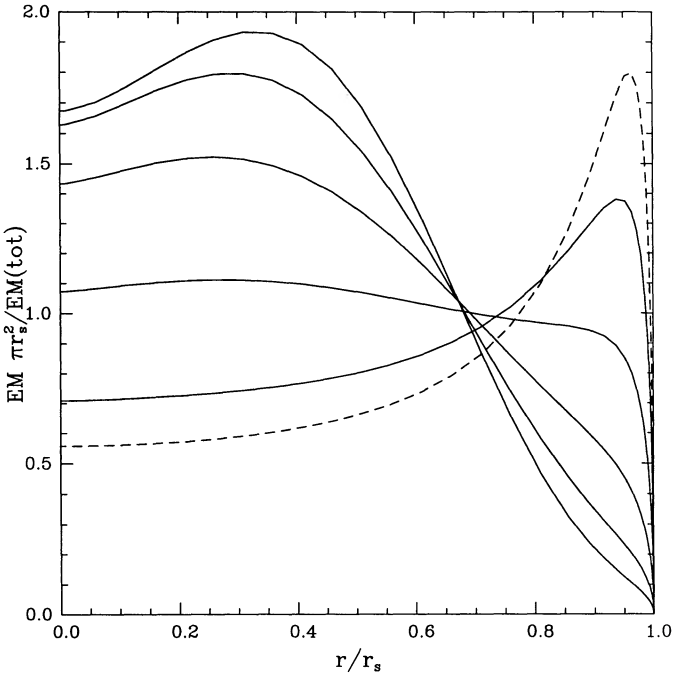

FIG. 4*b*

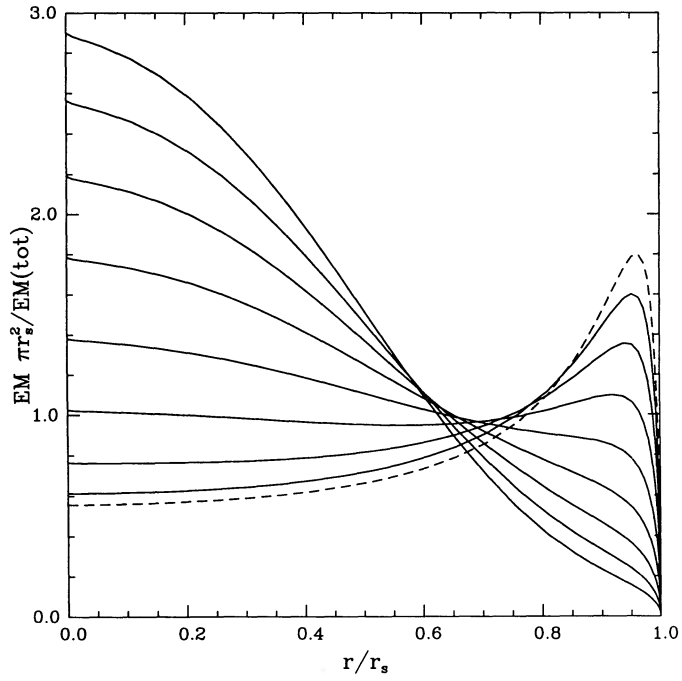

FIG. 4*c*

FIG. 4.—Normalized column emission measure vs. radius. (*a*) Same as Fig. 1*a*. (*b*) Same as Fig. 1*b*. (*c*) Same as Fig. 2.

and 2. We have chosen to plot the normalized surface brightness,

$$\mathrm{EM}(b)\pi r_s^2 \Big/ \int_0^{r_s} db\ \mathrm{EM}(b)2\pi b$$

this means that the profiles in Figure 4 represent a sequence in which the total X-ray luminosity is fixed while the model parameters vary. For models in which the mean density of the ISM is dominated by clouds ($C = \rho_{c1}/\rho_1 > 1$) with moderately long evaporation time scales ($\tau = t_{\mathrm{evap}}/t > 1$), the X-ray surface brightness can be much larger in the center than in the usual Sedov solution; the surface brightness can, in fact, be peaked in the center so that the SNR would not look shell-like at all. Long et al. (1990) confirm this conclusion with more detailed calculations of the X-ray emission.

As an indication of the spectrum of the X-ray emission, we can calculate the EM–weighted temperature $\langle T \rangle$:

$$\langle T \rangle = \frac{1}{\mathrm{EM}_{\mathrm{tot}}} \int_0^{r_s} dr 4\pi r^2 n^2 T = T_s \left[\int_0^1 dx x^2 g(x) f(x) \right] \Big/ \left[\int_0^1 dx x^2 g(x)^2 \right], \tag{23}$$

where

$$T_s = \frac{2(\gamma - 1)}{(\gamma + 1)^2} \frac{\mu m_{\mathrm{H}}}{k} V_s^2 \tag{24}$$

is the temperature at the shock. The variation of $\langle T \rangle / T_s$ with model parameters is given in Tables 3 and 6. Note that in these tables, as for the figures, we have explicitly included the scaling of T_s with K so that the values of $\langle T \rangle$ for different parameters can be compared directly. The temperature drops as the amount of evaporated mass increases; this is mainly due to the decrease in the shock velocity V_s due to the decreasing value of K (eq. [6]; Tables 1 and 6). We have also calculated the variation of $\langle T \rangle$ with impact parameter; it is quite flat and typically varies by less than 30% across the diameter of the SNR.

It may be worthwhile to describe briefly how one might derive model parameters from X-ray observations of a SNR. The fundamental observational parameters are the radius r_s, the luminosity L_x, and the surface brightness distribution. (The first two parameters depend on the SNR distance, which may be poorly known.) From the radial brightness distribution one can determine approximate values of C and τ; it is generally easiest to consider first the one-parameter models (Fig. 4*c*) and then, if necessary, to generalize to the full two-parameter models (Figs. 4*a*–4*b*). For given values of C and τ, the gas density in the ICM just outside the shock is (from eq. [21]).

$$n_1 = 2.5\ \mathrm{cm}^{-3} \left(\frac{L_x}{10^{35}\ \mathrm{ergs\ s}^{-1}} \right)^{1/2} \left(\frac{r_s}{\mathrm{pc}} \right)^{-3/2} \left(\frac{\Lambda_x}{1 \times 10^{-22}} \right)^{-1/2} Q^{-1/2} \left(1 + \frac{C}{1 + \tau} \right)^{-1}, \tag{25}$$

where Q comes from Table 2 or 6. The age of the SNR can then be derived from equation (8):

$$t = 15\ \mathrm{yrs} \left[\frac{K}{K(\mathrm{Sedov})} \right]^{-1/2} n_1^{1/2} \left(\frac{r_s}{\mathrm{pc}} \right)^{5/2} \left(\frac{E}{10^{51}\ \mathrm{ergs}} \right)^{-1/2}, \tag{26}$$

where $K/K(\mathrm{Sedov})$ comes from Table 1 or 6. Note that without hard X-ray measurements it is not possible to constrain the plasma temperature very closely, because the X-ray spectrum is strongly affected by nonequilibrium ionization and the total soft X-ray emissivity depends rather weakly on the temperature (Hamilton, Sarazin, & Chevalier 1983). The total mass of X-ray emitting gas is

$$M_x = \int_0^{r_s} 4\pi r^2 \rho\, dr = 4\pi r_s^3 \rho_s \int_0^1 dx x^2 g(x) = 0.10\ M_\odot\, n_1 \left(\frac{r_s}{\mathrm{pc}} \right)^3 \left(1 + \frac{C}{1 + \tau} \right) G\,.$$

where the mass integral G is tabulated in Tables 4 and 6. As for the X-ray luminosity, a heuristic model of the evaporated mass has been divided into the integral to remove most of the strong variation with the model parameters.

Throughout this section we have included only emission from the ICM. However, the gas near the evaporating clouds could also be a significant source of X-ray emission. That gas will be cooler than the ICM but will also be denser. The outer parts of the evaporating flows that are still hot enough to emit X-rays will contribute a significant amount of X-ray emission if the volume emission measure of that gas is comparable to the emission measure of the ICM. The X-ray emissivity of the evaporating gas will be strongly affected by nonequilibrium ionization effects, which may enhance its emissivity compared to the ICM. On the other hand, the X-ray emission from the evaporating flows will probably be softer than that from the ICM, so it will be more strongly absorbed by intervening interstellar matter and so will be harder to observe.

McKee & Cowie (1977) discussed the total emissivity of the gas near evaporating clouds. They show that the radiative cooling of the intercloud gas is enhanced by a factor $\beta \sim 10^3$–$10^4 f$, where f is the cloud filling factor. This implies that for reasonable values of f the total radiative losses in a cloudy medium may be dominated by the emission of the evaporating clouds. However, much of this radiation comes from gas with $T \sim 10^5$ K and does not contribute to the X-ray emission. McKee & Cowie did not calculate the enhancement of radiative emission as a function of wavelength. An accurate calculation of the X-ray emission from evaporating clouds would be of considerable interest.

3.2. *Infrared Emission*

SNRs also emit infrared radiation through the collisional heating of dust grains embedded in the hot gas (Ostriker & Silk 1973; Draine 1981; Braun 1987; Dwek 1987; Graham et al. 1987; Dwek et al. 1987). The IR to X-ray luminosity ratios from SNRs with

evaporating clouds will be similar to those from the usual Sedov models. However, the very different density distribution within the SNRs discussed in this paper will lead to different IR morphologies. Dust will certainly be present both in the evaporating gas that is boiling off the cold clouds and in the lower density intercloud medium. In either case, the lifetime of the dust against destruction by sputtering is long compared to typical SNR ages. In gas with a temperature $T \gtrsim 10^6$ K and electron density n_e (cm^{-3}), the lifetime of a grain of radius $a(\mu\text{m})$ is $\sim 10^6 a/n_e$ yr (Draine & Salpeter 1979). Even a small grain ($a = 0.01$ μm) in a high-density SNR ($n_e = 1$ cm^{-3}) can last for 10^4 yr. Dwek & Werner (1981; see also Dwek 1981 and Draine 1981) showed that a grain embedded in this gas is heated to an equilibrium temperature

$$T_{\rm gr} = 0.272 \text{ K} \left[\frac{n_e h(z)}{a}\right]^{0.2} T^{0.3} \tag{28}$$

and has a luminosity

$$L_{\rm gr} = 3.8 \times 10^{-15} a^3 T_{\rm gr}^5 \text{ ergs s}^{-1} , \tag{29}$$

where $z = 2.7 \times 10^8 a^{2/3}/T(\text{K})$ and $h(z)$ is an efficiency factor:

$$\begin{aligned} h(z) &= 1 , & z > 4.5 ; \\ &= 0.37 z^{0.62} , & z > 1.5 ; \\ &= 0.27 z^{1.50} , & \text{otherwise} . \end{aligned} \tag{30}$$

For the young and middle-aged SNRs we are considering, the high T limit ($z < 1.5$) is generally applicable; then we can derive the following simple results:

$$\begin{aligned} T_{\rm gr} &= 70.8 n_e^{1/5} \text{ K} ; \\ L_{\rm gr} &= 6.8 \times 10^{-6} n_e a^3 \text{ ergs s}^{-1} = 5.4 \times 10^5 n_e m_{\rm gr} \text{ ergs s}^{-1} , \end{aligned} \tag{31}$$

where $m_{\rm gr}$ is the grain mass in grams. Here we have used 3 g cm^{-3} as the density of grains.

This is a very nice result. First, the temperature of the dust depends weakly on the density of the hot gas and on nothing else. Recall that the density profile in our similarity solution does not change with time (eqs. [3a] and [4]; this is also true for the standard Sedov solution). Consequently, the dust temperature profile is time-independent. The peak wavelength of this IR radiation is $\lambda_{\rm IR} = 41 n_e^{-1/5}$ μm, which is very similar to the IR emission observed from the young SNRs Kepler, Tycho, and Cas A (Braun 1987).

Second, the luminosity of a collection of grains depends only on the gas density and on the total mass of dust; it is independent of the size distribution of the dust grains. This implies that the total IR luminosity will depend on the dust-to-gas ratio $\rho_{\rm gr}/\rho$ but on no other properties of the dust.

The total IR emission from a SNR is then just the sum of the luminosity of all the embedded grains. If we integrate over our density distribution and use a dust-to-gas ratio of d, then the total emission is

$$L_{\rm IR} = \int_0^{r_s} dr 4\pi r^2 5.4 \times 10^5 n_e \rho_{\rm gr} \text{ ergs s}^{-1} = 2.0 \times 10^{36} \text{ ergs s}^{-1} \left(\frac{d}{0.01}\right)\left(\frac{r_s}{1 \text{ pc}}\right)^3 n_1^2 \left(1 + \frac{C}{1+\tau}\right)^2 Q . \tag{32}$$

Notice that the dimensionless integral Q here is the same as that for the total emission measure (eq. [2]) and is given as a function of model parameters in Tables 2 and 6. The ratio of the IR luminosity to the X-ray luminosity is independent of the model parameters:

$$\frac{L_{\rm IR}}{L_x} = 120 \left(\frac{d}{0.01}\right)\left(\frac{10^{-22} \text{ cm}^3 \text{ ergs s}^{-1}}{\Lambda_x}\right) . \tag{33}$$

This ratio is similar to that found using more detailed calculations (Dwek 1987) and is in reasonable agreement with observations of SNRs (Graham et al. 1987; Dwek et al. 1987). Because it depends mainly on atomic physics, it is largely independent of the SNR model; however, the X-ray emissivity is affected by nonequilibrium ionization effects, which do depend on the SNR structure (Hamilton, Sarazin, & Chevalier 1983).

In the calculation above we have ignored the IR emission from the evaporating flows near the surfaces of clouds. Dwek (1981) calculated the infrared emission from a single evaporating cloud embedded in hot gas. He used a simple approximation to CM's evaporation solution that is appropriate very close to the surface of the cloud and neglected emission far out in the flow. From his calculation it is easy to show that the total IR emission from the remnant is dominated not by the small amount of dense gas at the surface of the clouds but by the tenuous, hot gas that fills almost the entire volume of the remnant. Further, the mean IR emission per unit volume near the clouds is *smaller* than the mean IR emissivity in the intercloud medium; thus, with observations of sufficient angular resolution and sensitivity there would appear to be *holes*, not bright spots, in the IR emission in the vicinity of clouds. Evaporating clouds increase the IR luminosity of a SNR by increasing the mean density of hot gas in the interior of the remnant, but as long as the volume filling factor of evaporating clouds is small, the IR emission associated with the evaporating flows of individual clouds is negligible.

One prediction of our model is that the morphology of the IR emission should be similar to the morphology of the X-ray emission. Unfortunately, the IR emission from those SNRs known to have centrally peaked, thermal X-ray emission (Long et al. 1990) is not bright enough to have been detected by the *IRAS* satellite; however, in the future we may hope to observe more SNRs to test this prediction.

3.3. *Optical Emission*

Optical line emission from SNRs can originate only in high-density gas clouds that are much cooler than the bulk of the SNR gas ($T \sim 10^4$ K instead of 10^7 K, $n \sim 10^2$ cm^{-3} instead of 0.1 cm^{-3}). In the standard picture of SNR evolution, this high-density gas is interpreted as clouds of interstellar or circumstellar matter that are shock-heated to a few times 10^4 K. Such shocked gas has a distinctive optical spectrum, featuring especially strong emission lines of [S II], [O II], [O III], and [N II] relative to Hα (e.g., Dopita et al. 1984; Fesen, Blair, & Kirshner 1985).

In our models optical emission may originate via the same mechanism; however, there may also be significant optical emission from the surfaces of the evaporating clouds. We have not calculated the complete optical emission characteristics of the clouds in our models since the emission depends rather strongly on the details of the flow and the full calculation is beyond the scope of this paper. However, we do calculate the contributions to the Hα luminosity expected from evaporating clouds.

When neutral gas is quickly raised to a high temperature, as in evaporating flows, neutral hydrogen atoms emit collisionally excited line radiation; typically each H atom emits ~0.1–0.3 Hα photons before it is ionized (Chevalier & Raymond 1978; Raymond et al. 1983; Cox & Raymond 1985). This implies that the collisional Hα from an evaporating cloud is simply proportional to the evaporation rate from the cloud:

$$L_{\rm cloud}({\rm H}\alpha) = F h\nu_{{\rm H}\alpha} \frac{X_{\rm H} \dot{m}_c}{m_{\rm H}} , \tag{34}$$

where $F \simeq 0.1$–0.3 is the number of Hα photons per ionization and $X_{\rm H} = 0.75$ is the mass fraction of hydrogen. The ratio of Hα photons produced by collisional excitation to those produced by recombination will vary from cloud to cloud, with recombination being relatively more important in clouds with higher mass loss rates [roughly $L_{\rm coll}({\rm H}\alpha)/L_{\rm recom}({\rm H}\alpha) \propto \dot{m}_c^{-1/2}$]. Estimates based on the evaporation rates from Cowie & McKee (1977) using plausible cloud parameters indicate that the collisionally excited Hα will dominate the recombination Hα by an order of magnitude.

Therefore, the total Hα luminosity from evaporating clouds within the SNR can be computed directly from the evaporation rate used for the similarity solution:

$$L_{{\rm H}\alpha} = h\nu_{{\rm H}\alpha} F X_{\rm H}/m_{\rm H} \int_0^{r_s} dr 4\pi r^2 j(r) = h\nu_{{\rm H}\alpha} F X_{\rm H} 4\pi r_s^3 j_s/m_{\rm H} \int_0^1 dx x^2 k(x) . \tag{35}$$

If we substitute the results from § 2 we find

$$\begin{aligned} L_{{\rm H}\alpha} &= 5 h\nu_{{\rm H}\alpha} F \frac{X_{\rm H}}{m_{\rm H}} \frac{C}{\tau} [\pi \rho_1 r_s (\gamma + 1) K E]^{1/2} \int_0^1 dx x^2 k(x) \\ &= 4 \times 10^{35} \text{ ergs s}^{-1} \left(\frac{F}{0.3}\right) n_1^{1/2} \left(\frac{r_s}{1 \text{ pc}}\right)^{1/2} \left(\frac{E}{10^{51} \text{ ergs}}\right)^{1/2} \left[\frac{C}{\tau} K^{1/2} \int_0^1 dx x^2 k(x)\right] \\ &= 4 \times 10^{35} \text{ ergs s}^{-1} \left(\frac{F}{0.3}\right) n_1^{1/2} \left(\frac{r_s}{1 \text{ pc}}\right)^{1/2} \left(\frac{E}{10^{51} \text{ ergs}}\right)^{1/2} S . \end{aligned} \tag{36}$$

The expression in brackets (the "evaporation integral" S) is tabulated as a function of C and τ in Tables 5 and 6. For evaporation-dominated SNRs, $L_{{\rm H}\alpha}$ can be larger than either L_x or $L_{\rm IR}$. However, this predicted Hα luminosity is smaller by a factor of a few than the luminosity observed by Long et al. (1990) for the remnant W28, which lends credence to our suggestion that the X-ray morphology of this and similar SNRs is determined by evaporating clouds. The observed Hα luminosity sets an upper limit to the evaporation rate that is consistent with our model.

McKee, Cowie, & Ostriker (1978) calculated the Hα emission for an evaporating cloud when the conduction is not saturated. In that case the Hα emission is dominated by an H II region produced on the surface of the cloud by ionizing photons generated in the evaporating flow. However, McKee & Cowie (1977) found that the ionized region is not important when the conduction becomes saturated; in that case we believe that the Hα is dominated by gas in the evaporating flow, as we have assumed above.

The ratio of forbidden line emission (e.g., [S II] λλ6716, 6731) to Hα depends on the cloud evaporation rate. To calculate the optical line ratios accurately, then, we would have to average over the ensemble of evaporating clouds. We shall not attempt such a calculation in this paper because it requires a far more detailed model of the evaporation than we have used in this paper. Such a calculation would be of considerable interest, however, since evaporating clouds might have rather unusual line ratios that would permit definitive tests of the model we propose here.

Although we have not calculated the [S II] λ6716, 6731 line emission, we believe that this density-sensitive line ratio should be near its low-density limit in evaporating flows. The [S II] emission may be reduced if the density in the cloud is high enough for collisional de-excitation of the forbidden [S II] transition. This becomes important for n greater than 10^2 cm^{-3} $(T/10^4 \text{ K})^{1/2}$ (Osterbrock 1974). Certainly in the high-density gas near $T \sim 10^4$ K this limit may be exceeded in dense clouds; note also that in an ensemble of clouds with a range of densities the dense clouds will contribute the most line emission. However, S^+ is the dominant ion of sulfur for $T = 10^4$–10^5 K, and collisional de-excitation will not be important in the gas near $T = 10^5$ K unless the pressure in the gas exceeds $nT = 3 \times 10^7$ K cm^{-3}. Such high pressures will not be found except in the youngest and densest SNRs. It is likely that when collisional de-excitation is included the [S II] emission will be reduced by at most a factor of a few; it is also likely that the [S II] 6716:6731 line ratio will be near the low-density limit even if most of the Hα emission originates in much higher density gas. The latter is consistent with the observations of Long et al. (1990).

4. CONCLUSIONS

We have derived a new similarity solution that describes the evolution of supernova remnants expanding into a cloudy ISM. The model applies to SNRs which are between 10^3 and 2×10^4 years old; for such remnants the clouds evaporate by saturated conduction (Cowie & McKee 1977; Cowie, McKee, & Ostriker 1981). The solution has two dimensionless parameters: C, the ratio of the mass in clouds to the mass in the intercloud medium, and τ, the ratio of a typical cloud evaporation time to the age of the remnant. For the similarity solution to exist τ must be constant; we have found that realistic cloud evaporation rates scale in very nearly the required way. In many cases we can use the one-parameter family of solutions derived by fixing C/τ and letting $\tau \rightarrow \infty$; the one-parameter solutions closely resemble the two-parameter solutions in most of their essential characteristics.

We have summarized the X-ray, infrared, and optical emission characteristics of these remnants. Their X-ray morphologies may be very different from ordinary shell-like SNRs, including possibly having X-ray emission that is peaked in the center like the remnants discussed by Long et al. (1990). The IR luminosity of a remnant is determined by its total volume emission measure; the evaporating clouds do not contribute significant additional IR radiation. The morphology of the IR emission is predicted to be similar to that of the X-ray emission; the IR luminosity is expected to be ~ 120 times the X-ray luminosity, which is consistent with the upper limits from the *IRAS* satellite for filled-center SNRs. The optical spectrum of the evaporating clouds should be similar to that of shocked gas, although some line ratios could be distinctly different. The total Hα luminosity from evaporating clouds predicted by this model is less than that observed for SNRs with centrally peaked thermal X-ray emission (Long et al. 1990); this model could have been ruled out if the predicted Hα luminosity exceeded the observed luminosities. The Hα luminosity is larger than either the IR or the X-ray luminosities. A detailed calculation of the X-ray and optical line emission from evaporating clouds would be of great utility in testing this model against the observations.

We would like to thank Chris McKee for many useful comments. This work was supported by NASA SADAP grant NAG-8-677.

REFERENCES

Braun, R. 1987, A&A, 171, 233
Chevalier, R. A. 1982, ApJ, 258, 790
Chevalier, R. A., & Raymond, J. C. 1978, ApJ, 225, L27
Chièze, J. P., & Lazareff, B. 1981, A&A, 95, 194
Cowie, L. L. 1977, ApJ, 215, 226
Cowie, L. L., & McKee, C. F. 1977, ApJ, 211, 135 (CM)
Cowie, L. L., McKee, C. F., & Ostriker, J. P. 1981, ApJ, 247, 908 (CMO)
Cox, D. P., & Edgar, R. J. 1983, ApJ, 265, 443
Cox, D. P., & Raymond, J. C. 1985, ApJ, 298, 651
Dopita, M. A., Binette, L., D'Odorico, S., & Benvenuti, P. 1984, ApJ, 276, 653
Draine, B. T. 1981, ApJ, 245, 880
Draine, B. T., & Salpeter, E. E. 1979, ApJ, 231, 77
Dwek, E. 1981, ApJ, 246, 430
———. 1987, ApJ, 322, 812
Dwek, E., Petre, R., Szymkowiak, A., & Rice, W. L. 1987, ApJ, 320, L27
Dwek, E., & Werner, M. W. 1981, ApJ, 248, 138
Fesen, R. A., Blair, W. P., & Kirshner, R. P. 1985, ApJ, 292, 29
Graham, J. R., Evans, A., Albinson, J. S., Bode, M. F., & Meikle, W. P. S. 1987, ApJ, 319, 126
Hamilton, A. J. S., Sarazin, C. L., & Chevalier, R. A. 1983, ApJ, 51, 115
Long, K. S., Blair, W. P., White, R. L., & Matsui, Y. 1991, ApJ, 373, 567
McKee, C. F. 1982, in Supernovae: A Survey of Current Research, ed. M. J. Rees & R. J. Stoneham (Dordrecht: Reidel), p. 433
McKee, C. F., & Cowie, L. L. 1977, ApJ, 215, 213
McKee, C. F., Cowie, L. L., & Ostriker, J. P. 1978, ApJ, 219, L23
McKee, C. F., & Ostriker, J. P. 1977, ApJ, 218, 148
Osterbrock, D. E. 1974, Astrophysics of Gaseous Nebulae (San Francisco: W. H. Freeman)
Ostriker, J. P., & McKee, C. F. 1988, Rev. Mod. Phys., 60, 1
Ostriker, J. P., & Silk, J. 1973, ApJ, 184, L113
Pye, J. P., Becker, R. H., Seward, F. D., & Thomas, N. 1984, MNRAS, 207, 649
Raymond, J. C., Blair, W. P., Fesen, R. A., & Gull, T. R. 1983, ApJ, 275, 636
Sedov, L. 1959, Similarity and Dimensional Methods in Mechanics (New York: Academic)
Sgro, A. G. 1975, ApJ, 197, 621
Smith, A., Jones, L. R., Watson, M. G., Willingale, R., Wood, N., & Seward, F. D. 1985, MNRAS, 217, 99
Woltjer, L. 1972, ARA&A, 10, 129